Wind-Generated Current and Phase Speed of Wind Waves[1]

OMAR H. SHEMDIN

Dept. of Coastal and Oceanographic Engineering, University of Florida, Gainesville 32601

(Manuscript received 17 February 1972, in revised form 1 May 1972)

ABSTRACT

Measurements of drift were made in a wind and wave facility at different elevations below the mean water level. The drift profiles were obtained for reference wind speeds, $U_r=3.1$, 5.7 and 9.6 m sec^{-1}. The measurement technique involved tracing the movement of small paper disks which were soaked in water to become neutrally buoyant at the elevation of release. A logarithmic drift profile is proposed. The water shear velocity U_{*_w} predicts a surface stress, $\tau_s=\rho_w U_{*_w}^2$, in agreement with that obtained from the wind shear velocity, $\tau_s=\rho_a U_{*_a}^2$, where ρ_a and ρ_w refer to air and water densities, respectively.

The influence of wind on phase speeds of waves was investigated by solving the first-order perturbation problem of the coupled shear flows in air and water. The air velocity profile was described by a logarithmic distribution and the drift profile was described by the proposed drift profile. Adequate agreement is found between the calculated and measured phase speed using Doppler radar in the wavenumber range 1.9–10 cm^{-1}. In the wavenumber range 0.05–0.5 cm^{-1}, measurements of phase speeds were obtained by using two wave gages. The waves were mechanically generated without wind and the wave gages were spaced to obtain coherent signals. The wind was then allowed to blow over the waves and the distance between wave gages was increased to maintain coherence. The wavelength and frequency were obtained from the distance between the gages and from the generator frequency, respectively. The measured phase speeds were found to increase with wind speed consistent with theoretical computations.

1. Introduction

Wind action over water generates both waves and surface drift. Waves contribute to the surface drift through Stokes mass transport. A portion of the total rate of momentum transfer to the water is through the normal stress acting on the disturbed surface and the other portion is due to the tangential stress which contributes, at least in part, to the surface drift. The details of the transfer of momentum and energy from air to water by the normal and tangential stresses are not completely understood yet.

The purpose of this investigation is to shed light on the interaction between the wind-generated waves and the wind-induced current. That such an interaction exists can be observed in a wind and wave facility in which waves can be generated mechanically. In the absence of wind, mechanical waves with a preselected length can be generated and detected by two wave gages spaced an integral number of wavelengths apart. The simultaneous wave records under these conditions are coherent. When wind is allowed to blow over the mechanically generated waves the wave records exhibit a phase shift which increases with wind speed. The experimental and analytical results of this study suggest that surface drift induced by wind alters significantly the dispersion relationship for small-amplitude waves.

Previous investigations of surface drift were obtained by Van Dorn (1953) in a pond and by Keulegan (1951), Wu (1968), Plate and Trawle (1970) and Wright and Keller (1971) in the laboratory. The first two observers found the surface drift to be about 3% of the wind speed under turbulent conditions. The surface drift was found to be independent of surface waves which they were able to show by suppressing the waves by spreading detergent over the water surfaces. The other investigators recorded surface drifts in the range 2.5–4.0% of the wind speed.

Observations by Francis (1951), Cox (1958), Hide and Plate (1966) and Plate and Trawle (1970) all indicated phase speeds of wind-generated waves greater than the calculated values based on the linear wave theory. The difference was found to be greater than that due to the finite amplitude of the waves and was accordingly attributed to the surface drift. An analytical solution by Plate and Trawle based on a linear drift profile below the surface was found to produce unsatisfactory agreement with observations. They concluded that the need existed for a careful computation of phase speeds based on a reasonable drift profile below the interface.

An interesting computation of surface drift based on Stokes mass transport was carried out by Kenyon

[1] Paper presented at the Conference on the Interaction of the Sea and the Atmosphere, 1–3 December 1971, Ft Lauderdale, Fla.

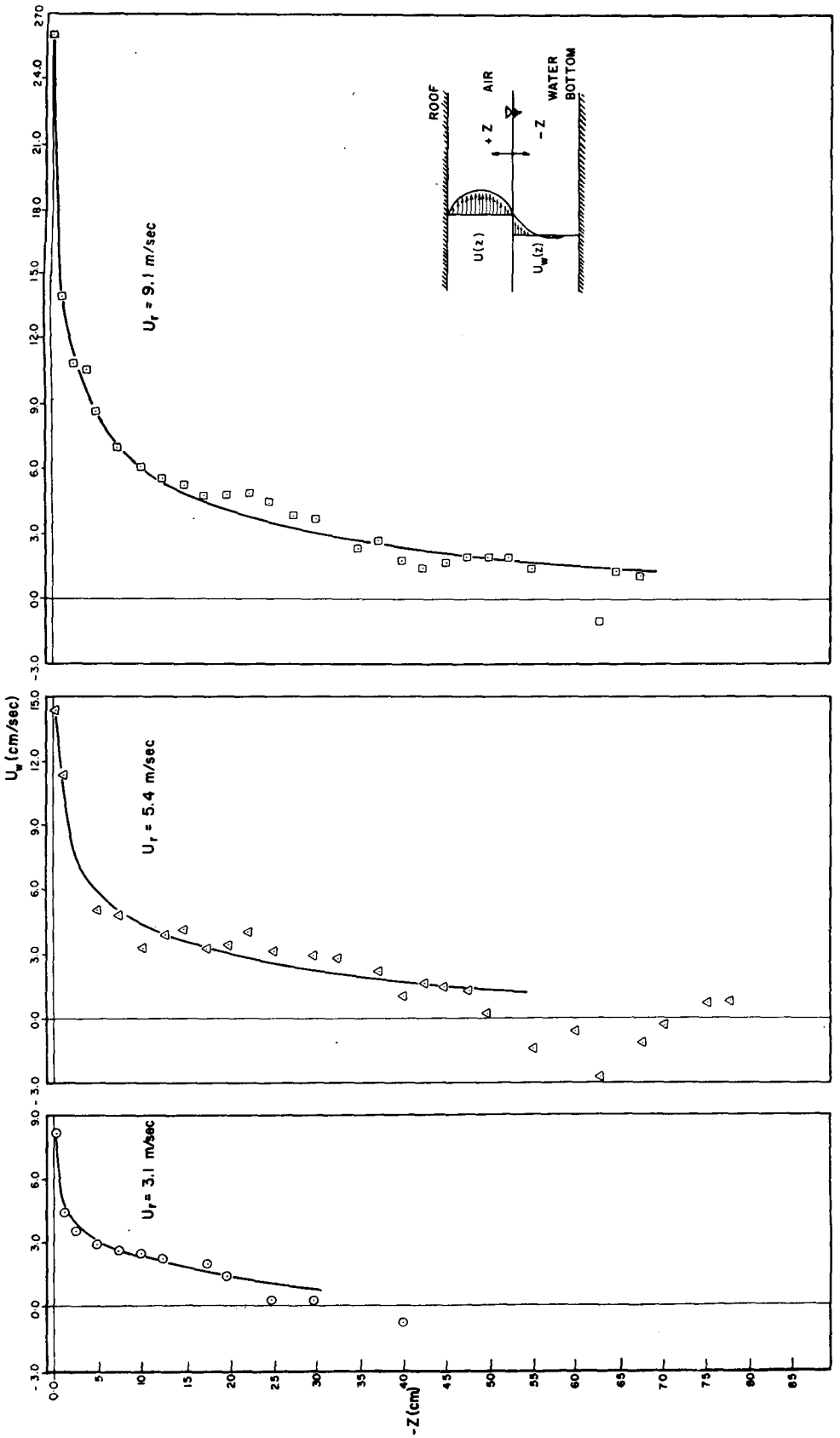

FIG. 1. Wind-generated drift profiles associated with the three reference air speeds.

(1969) for a fully developed sea. The computation suggests that the entire wind stress is supported by waves in a fully developed sea. However, fetch-limited laboratory and field observations do not verify this result.

2. Laboratory experiments

a. The wind-wave facility

The wind and wave facility at the University of Florida was used to conduct experiments on wind-generated drift and phase speed of waves under the influence of wind-generated drift. The facility is described by Lai and Shemdin (1971). Briefly, the wave channel is 1.83 m wide and 45.7 m long, and is divided into two bays of equal width. The height of the facility is 1.93 m and the water depth is maintained at 91.5 cm by a small water pump. One bay is provided with a roof and is used as a wind channel. The wind intake is modified to produce a turbulent flow regime throughout in the wind channel. Waves can be generated mechanically by an electrohydraulic system. The wave energy is absorbed at the down-wind end of the tank by baskets mounted on a steel ramp and filled with stainless steel turnings.

The wind velocity profile over the water surface was measured by a standard pitot-static tube manufactured by United Sensors, Inc., and a sensitive differential pressure transducer. The velocity profiles near the air-water interface were found to follow a logarithmic distribution as shown by Lai and Shemdin (1971). From the slopes of the logarithmic distributions the shear velocity U_{*_a} was obtained and used to evaluate the boundary shear stress at different wind speeds.

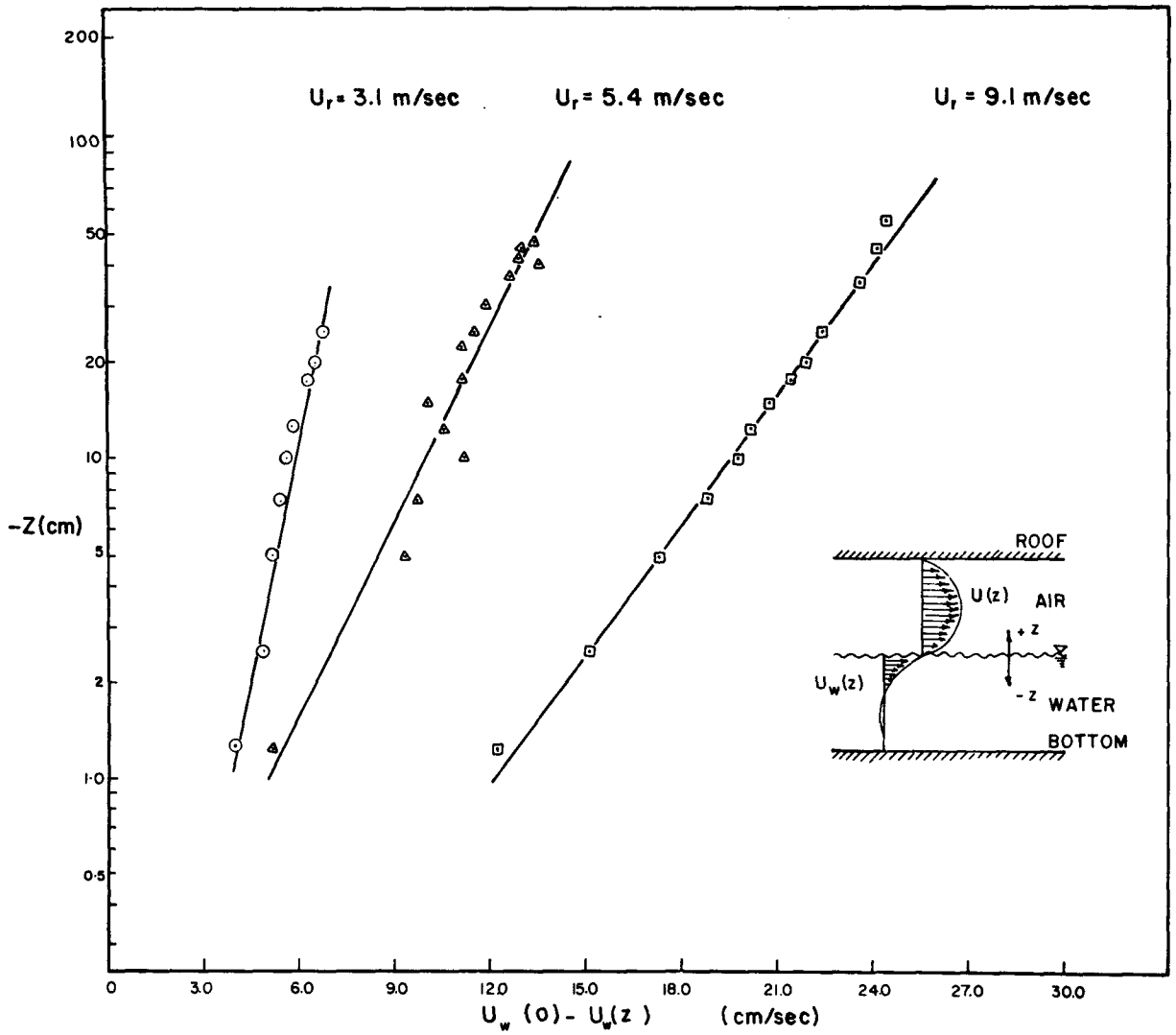

FIG. 2. Logarithmic fit of the wind generated drift profiles.

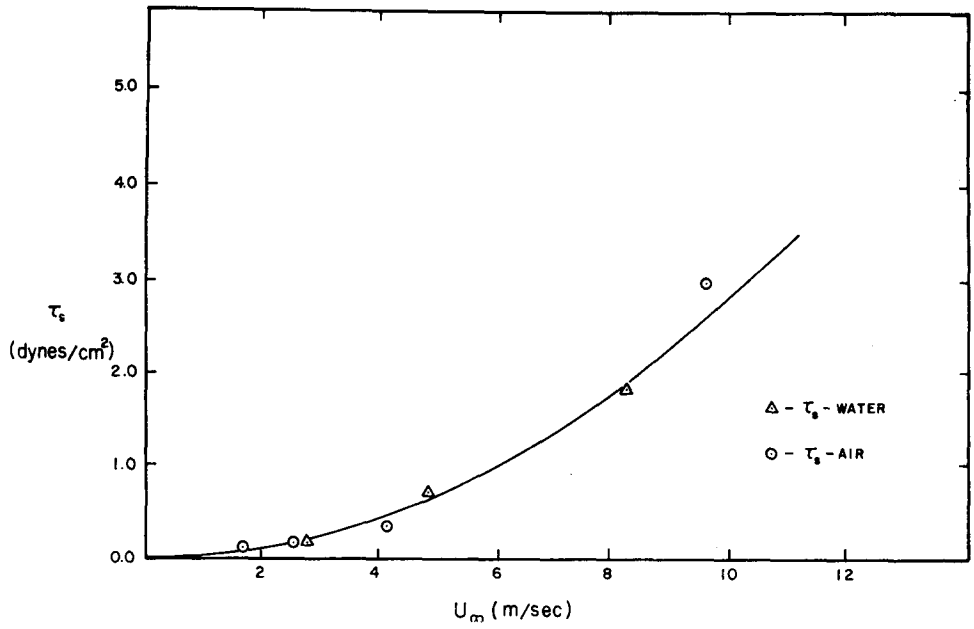

FIG. 3. Surface stress obtained from both the air and the drift profiles.

b. Wind-generated drift profile

The drift of neutrally buoyant particles below the surface was measured by using small paper disks 6 mm in diameter. The disks were obtained by a standard paper hole puncher. When soaked in water for a few seconds the paper disks became neutrally buoyant and followed the wind-induced drift. It was found desirable to soak the disks at the elevation of the release since a vertical temperature gradient existed in the water which affects the buoyancy of the disks. Normally a few disks were released, some ascended and other descended in the flow but invariably a few remained at the elevation of the release and drifted horizontally. Particle speeds of ten disks were averaged at each elevation to obtain a mean value for that elevation.

The drift profiles for three reference wind speeds, $U_r=3.1$, 5.4 and 9.1 m sec^{-1}, are shown in Fig. 1. The reference probe is located at 183 cm downstream of the air intake and 16.5 cm below the roof plate and is used to insure repeatability of experiments. The drift profiles exhibit a sharp gradient immediately below the surface and follow a logarithmic distribution when plotted downward with respect to the surface as shown in Fig. 2. A logarithmic profile of the form

$$U_w(0)-U_w(z)=\frac{U_{*_w}}{\kappa}\ln\left(\frac{z}{z_{0w}}\right), \tag{1}$$

is proposed where $U_w(0)$ is the surface drift, $U_w(z)$ the drift at elevation z below the surface, κ the universal von Kármán constant, and z_{0w} a roughness height. Such a profile was observed by Bye (1967) to describe the ocean drift measurements reasonably well. This profile has a number of desirable features: (i) it has an analogous form to the profile associated with a rough turbulent boundary layer past a rigid boundary and suggests that the drift current is turbulent in nature; (ii) it yields a shear velocity U_{*_w} which provides an independent method to estimate the surface stress τ_s defined by

$$\tau_s=\rho_w U_{*_w}{}^2, \tag{2}$$

where ρ_w is the water density; and (iii) it provides a shear profile to investigate analytically the properties of the wind-generated waves superimposed on the wind-generated drift.

The surface stress τ_s can also be estimated from the wind velocity profiles by the relationship

$$\tau_s=\rho_a U_{*_a}{}^2, \tag{3}$$

where ρ_a is the air density and U_{*_a} is obtained by fitting the log relation (17) to the wind profile. The surface stress values obtained using both wind and drift profiles are compared in Fig. 3 for different free stream (maximum at station in the wind tunnel) wind speeds U_∞. The three drift profiles shown in Fig. 2 were used to obtain the surface stresses according to (2). Four other wind profiles corresponding to reference wind speeds $U_r=1.95$, 2.96, 4.57 and 10.66 m sec^{-1}, were available and were used to obtain the surface stress according to (3). The best fit curve through all the data is given by

$$\tau_s=2.45\times10^{-3}\rho_a U_\infty{}^2, \tag{4}$$

where the drag coefficient 2.45×10^{-3} is consistent with other laboratory measurements.

In a fully developed sea, it was suggested by Bye (1967) and Kenyon (1969) that the wind-induced drift is due primarily to Stokes mass transport S, given by

$$S=a_0^2\sigma k e^{-2kz}, \tag{5}$$

where a_0, σ and k are the wave amplitude, frequency and wavenumber, respectively. Integrating over the frequency range in a wave spectrum from σ_u (angular frequency corresponding to minimum wave speed under gravity and surface tension) to σ_L (angular frequency corresponding to spectrum peak), Bye obtained the following relationship for the surface drift $U_w(0)$:

$$U_w(0)=\frac{30}{\sigma_L}\ [\text{cm sec}^{-1}]. \tag{6}$$

The measured wind-wave spectrum peak for $U_r=9.1$ m sec^{-1} was found to correspond to $\sigma_L=12.56$ rad sec^{-1}. Using (6) the surface drift is computed to be 2.4 cm sec^{-1} which is one order of magnitude smaller than the

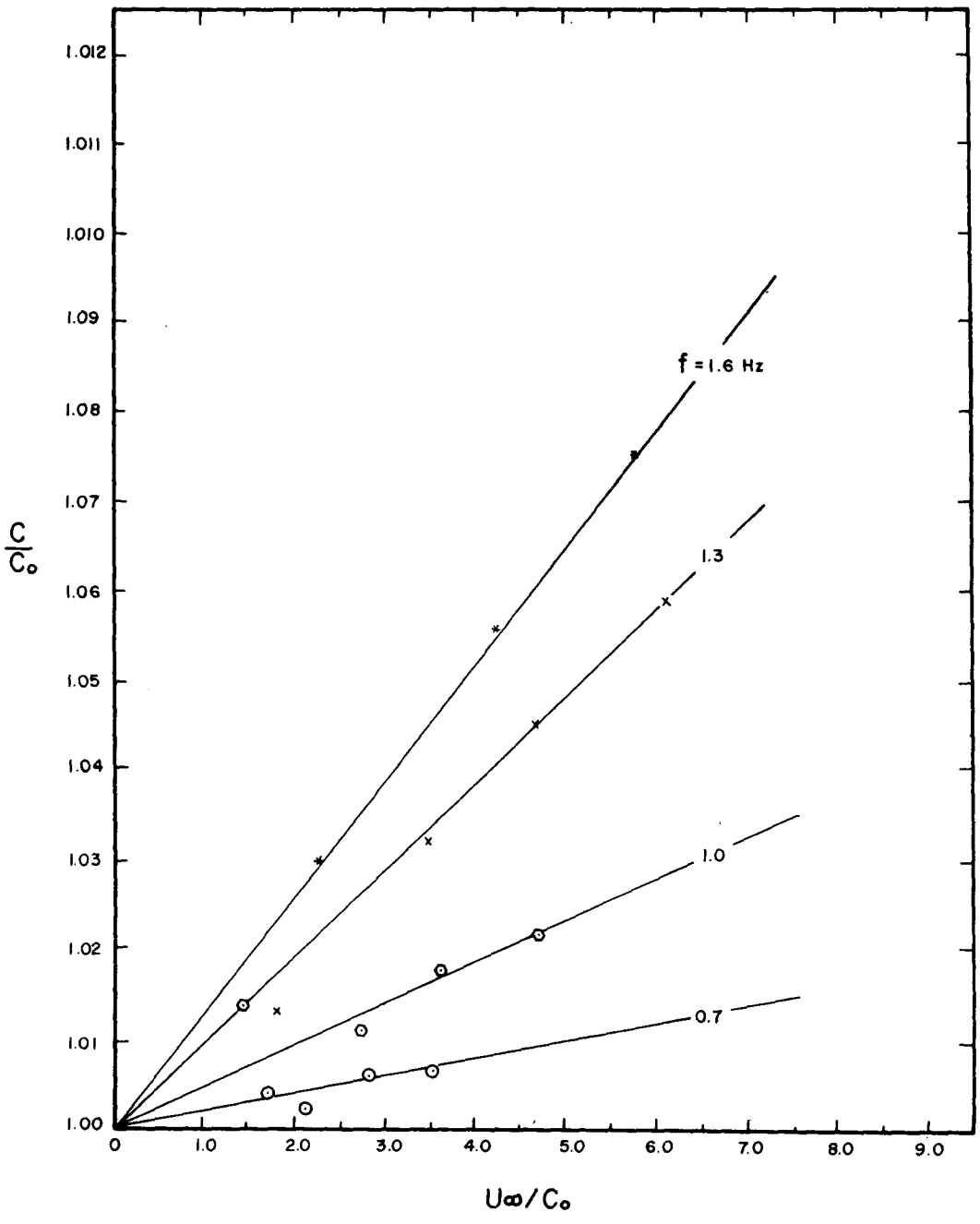

FIG. 4. Dependence of phase speed on wind speed U_∞.

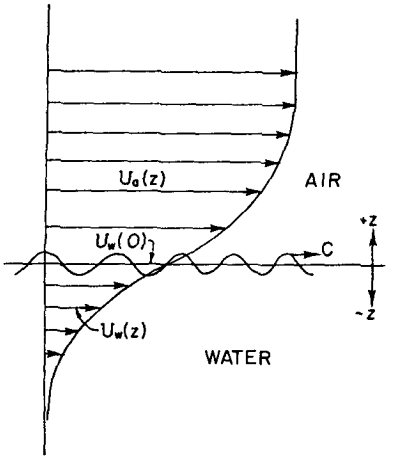

FIG. 5. Definition sketch.

measured value of 26.2 cm sec^{-1}. Some doubts remain regarding the mechanism of surface drift in the absence of wind. Longuet-Higgins (1960) estimated the vertical gradient of the drift at the surface to be twice the Stokes mass transport because of viscosity. This was disputed by Huang (1970), however. Regardless of the dominating mechanism, the above computation suggests that in a fetch-limited case the wind-generated drift is primarily due to the direct shear stress action of wind. This conclusion is consistent with the observations of both Keulegan (1951) and Van Dorn (1953) who found the surface drift to remain unchanged when wind-generated waves were suppressed by spreading detergent over the water surface. The surface drift, $U_w(0)$, for all the three cases shown in Fig. 1, was found to be 3% of the free stream velocity U_∞, and in agreement with the results of Keulegan and Van Dorn. More recently, drift measurements were obtained by Wu (1968) who reported a linear drift profile near the surface from which he found the surface drift to vary from 3.0–5.0% of U_∞. These drift profiles were measured in a layer 3.8 mm below the surface. Estimates of the surface stress based on such a linear gradient can be subject to errors due to the steep gradient near the surface which is perturbed by wind-generated ripples.

c. Phase speed of wind waves

As indicated in Section 1 the phase speeds of wind-generated waves were found by other investigators to be greater than values calculated on the basis of linear wave theory. In order to verify these results and to provide complete data for comparison with an analytical prediction (to be discussed in Section 3), measurements of phase speeds were obtained in the wind-wave facility by using mechanically generated waves and two capacitance wave gages. Initially no wind was allowed and the two wave gages were spaced an integral number of wavelengths apart to obtain a coherent signal. Then wind was allowed to blow over the water surface and one wave gage was moved away from the other until the signals became coherent again. The new distance between the wave gages was taken to represent an integral multiple of the mechanically generated wavelength in a current-wave field. From the wavelength and frequency the phase speed C was computed. This procedure was followed for waves with wavenumbers in the range 0.05–0.5 cm^{-1} and free stream velocity U_∞ from 0–8.0 m sec^{-1}. Both C and U_∞ were normalized with respect to C_0, defined by

$$C_0^2 = g/k + Tk/\rho_w, \tag{7}$$

where g is the gravitational constant and T the surface tension. The results are shown in Fig. 4 for different mechanically generated waves. It is noted that at high wind speeds the wind-generated waves drowned the mechanical wave signal and a phase averaging device was used to enhance the periodic wave signal and to suppress the random wind-generated ripples. Use was made of a signal averager Model 281 manufactured by Fabri-Tek Instruments, Inc.

The results of Fig. 4 suggest a linear relationship between c and U_∞. Other experimental results by Wright and Keller (1971) obtained for higher wavenumbers from Doppler spectra of radar backscattering from wind-generated waves indicate that the relationship between C and U_∞ need not be a linear one.

3. Linear coupling between wind and waves

The influence of the wind on the dispersion relation for simple harmonic waves is investigated here via a linear model similar to that of Miles (1957), which was concerned primarily with wave generation. The present formulation is not intended to improve the Miles' model for the air flow, by including the effects of viscosity and nonlinear terms (cf. Shemdin, 1969; Saeger and Reynolds, 1971), but rather to include the shear flow on the water side which has heretofore been neglected. It will be demonstrated that the inclusion of the water shear flow can significantly change the dispersion relationship for the waves in the presence of wind, particularly for capillary waves.

Attention is confined to the displacement η of the interface being of simple harmonic progressive form:

$$\eta = \mathrm{Re}[ae^{ik(x-ct)}]. \tag{8}$$

a. Equations of motion for flow below the interface

Considering a coordinate system defined in Fig. 5 where waves propagate in the positive x direction with crests parallel to the y direction, and z positive in the vertical direction, the equations of motion governing small perturbation of a two-dimensional shear flow $U_w(z)$ in an incompressible inviscid fluid with density

ρ_w are

$$\frac{\partial U_w}{\partial t}+U_w\frac{\partial U_w}{\partial x}+W_w\frac{\partial U_w}{\partial z}=-\frac{1}{\rho_w}\frac{\partial p_w}{\partial x}, \tag{9a}$$

$$\frac{\partial W_w}{\partial t}+U_w\frac{\partial W_w}{\partial x}=-\frac{1}{\rho_w}\frac{\partial p_w}{\partial z}-g, \tag{9b}$$

$$\frac{\partial U_w}{\partial x}+\frac{\partial W}{\partial z}=0, \tag{9c}$$

where U_w and W_w are the x and z components of the perturbation velocity and p_w is the perturbation pressure. Introducing a streamfunction defined as

$$U_w=\frac{\partial \psi_w}{\partial z}, \quad W_w=-\frac{\partial \psi_w}{\partial x},$$

and assuming ψ_w and p_w to have the same dependence on x and t as η in (8), i.e.,

$$\psi_w=\hat{\psi}_w e^{ik(x-ct)}, \quad p_w=\hat{p}_w e^{ik(x-ct)},$$

the following equations are obtained:

$$(U_w-C)\frac{\partial \hat{\psi}_w}{\partial z}-\hat{\psi}_w\frac{\partial U_w}{\partial z}=-\frac{\hat{p}}{\rho_w}, \tag{10a}$$

$$(U_w-C)\frac{\partial \hat{\psi}_w}{\partial x}=-\frac{1}{\rho_w}\frac{\partial \hat{p}}{\partial z}. \tag{10b}$$

Elimination of p_w yields the Rayleigh equation

$$(U_w-C)\frac{\partial^2 \hat{\psi}_w}{\partial z^2}-\left[k^2(U_w-C)+\frac{\partial^2 U_w}{\partial z^2}\right]\hat{\psi}_w=0. \tag{11}$$

The flow field below the interface may be obtained by solving (11) subject to the boundary conditions

$$\frac{\partial \hat{\psi}_w}{\partial z}=(U_w-C)\frac{\partial \eta}{\partial x} \text{ at } z=\eta\approx 0, \tag{12}$$

$$\hat{\psi}_w\to 0 \text{ as } z\to -\infty. \tag{13}$$

A convenient form for $U_w(z)$ is that given by (1).

b. Equations of motion for flow above the interface

For the lack of a superior model the inviscid model proposed by Miles (1957) will be adopted. The x and z components of the perturbation velocity are U_a and W_a, respectively, the perturbation pressure is p_a and the streamfunction is ψ_a. The following Rayleigh equation and boundary conditions can be derived in a manner similar to that for ψ_w:

$$(U_a-C)\frac{\partial^2 \hat{\psi}_a}{\partial z^2}-\left[k^2(U_a-C)+\frac{\partial^2 U_a}{\partial z^2}\right]\hat{\psi}_a=0, \tag{14}$$

$$\frac{\partial \psi_a}{\partial x}=(U_a-C)\frac{\partial \eta}{\partial x} \text{ at } z=\eta\approx 0, \tag{15}$$

$$\hat{\psi}_a\to 0 \text{ as } z\to +\infty. \tag{16}$$

The mean shear flow in air was assumed to have the form

$$U_a(z)=\frac{U_{*a}}{\kappa}\ln\frac{z}{z_{0a}}, \tag{17}$$

where z_{0a} is the roughness height.

c. Matching conditions at the interface

From the experimental results discussed previously it was found that the shear velocities in the air and in the water could be matched through the surface stress according to

$$\tau_s=\rho_a U_{*a}^2=\rho_w U_{*w}^2. \tag{18}$$

The normal pressures above and below the interface are matched according to

$$p_w-p_a+T\frac{\partial^2 \eta}{\partial x^2}=0 \text{ at } z=\eta\approx 0, \tag{19}$$

where T is the surface tension. The pressures are obtained from the equations of motion for the water and the air, respectively,

$$\frac{\hat{p}_w}{\rho_w}=\hat{\psi}_w\frac{\partial U_w}{\partial z}-(U_w-C)\frac{\partial \hat{\psi}_w}{\partial z}-ga \text{ at } z=0, \tag{20}$$

$$\frac{\hat{p}_a}{\rho_a}=\hat{\psi}_a\frac{\partial U_a}{\partial z}-(U_a-C)\frac{\partial \hat{\psi}_a}{\partial z}-ga \text{ at } z=0. \tag{21}$$

Eliminating the pressures in (19) yields

$$\frac{1}{ka}\left[\hat{\psi}_w\frac{\partial U_w}{\partial z}-(U_w-C)\frac{\partial \hat{\psi}_w}{\partial z}\right]=\frac{g}{k}\left(1-\frac{\rho_a}{\rho_w}\right)+\frac{Tk}{\rho_w}+\frac{1}{ka}\left[\hat{\psi}_a\frac{\partial U_a}{\partial z}-(U_a-C)\frac{\partial \hat{\psi}_a}{\partial z}\right] \text{ at } z=0. \tag{22}$$

d. Method of solution

Solution of the boundary value problem for the air was obtained numerically by Conte and Miles (1959). The surface pressure was defined as

$$\hat{p}_a=(\alpha_m+i\beta_m)\rho_a\left(\frac{U_{*a}}{\kappa}\right)^2 ka, \tag{23}$$

where α_m and β_m were evaluated from (21), i.e.,

$$(\alpha_m+i\beta_m)\left(\frac{U_{*a}}{\kappa}\right)^2=\frac{1}{ka}\left[\hat{\psi}_a\frac{\partial U_a}{\partial z}-(U_a-C)\frac{\partial \hat{\psi}_a}{\partial z}\right]-\frac{g}{k} \text{ at } z=0. \tag{24}$$

For given α_m and β_m Eq. (22) becomes

$$\frac{1}{ka}\left[\hat{\psi}_w\frac{\partial U_w}{\partial z}-(U_w-C)\frac{\partial\hat{\psi}_w}{\partial z}\right]=\frac{g}{k}+\frac{Tk}{\rho_w}+(\alpha_m+i\beta_m)\frac{\rho_a}{\rho_w}\left(\frac{U_{*a}}{\kappa}\right)^2. \quad (25)$$

It is noted that in the water the phase speed is mostly greater than U_w so that a critical layer is normally not present. Under these conditions $\hat{\psi}_w$ is real. For waves that grow or decay the phase speed is complex, i.e.,

$$C=C_r+iC_i.$$

Equating real and imaginary parts of (25) yields

$$\frac{1}{ka}\left[\hat{\psi}_w\frac{\partial U_w}{\partial z}-(U_w-C_r)\frac{\partial\hat{\psi}_w}{\partial z}\right]=\frac{g}{k}+\frac{Tk}{\rho_w}+\alpha_m\frac{\rho_a}{\rho_w}\left(\frac{U_{*a}}{\kappa}\right)^2 \text{ at } z=0, \quad (26a)$$

$$C_i\frac{\partial\hat{\psi}_w}{\partial z}=\beta_m\frac{\rho_a}{\rho_w}\left(\frac{U_{*a}}{\kappa}\right)^2 ka \text{ at } z=0. \quad (26b)$$

The propagation speed is given by C_r and was computed from (26a).

The procedure followed in computing C_r was an iterative one where an initial C_r value was assumed. The boundary value in the air was then solved to yield α_m, the boundary value problem in water was solved to yield $\hat{\psi}_w$ and its first derivative, and using (26a) a new value for C_r was computed. The computation was then repeated for the new C_r value. Solutions to the boundary value problems were obtained by numerical methods similar to the procedure followed by Conte and Miles (1959). The independent variables needed for a solution were U_{*a}, z_{0a} and z_{0w}. The experimental results exhibit considerable scatter in z_{0a} and z_{0w} depending on the velocity profile fit. In most cases it was found that both z_{0a} and z_{0w} were of the same order of magnitude. In the computations it was assumed that $z_{0a}=z_{0w}$ so that a complete computation could be obtained by simply specifying a logarithmic velocity profile for the air, i.e., specifying U_{*a} and z_{0a}. The surface drift velocity was experimentally found to be 3% of the free stream velocity or $0.6U_{*a}$. Convergence for C_r was normally obtained after 3–6 iterations depending on the input values of U_* and z_{0a}. Convergence was assumed when $\Delta C_r \leq 0.05C_r$ was achieved.

4. Results and discussion

Numerical computations were carried out for cases corresponding to the available experimental results. In the wavenumber range 1.9–15.8 cm^{-1} a comparison between the numerical predictions of the phase speed and the measured values by Wright and Keller (1971) are shown in Table 1. The difference in most cases is below 10%. It is noted that a free stream wind velocity of 7.9 m sec^{-1} can increase the minimum phase speed ($k=3.7$ cm^{-1}) by 100%. Convergence in this range of k was achieved readily. However, for the smaller wavenumbers which corresponded to the experimental results discussed in Section 2, convergence could not be obtained. Either overflow or underflow invariably

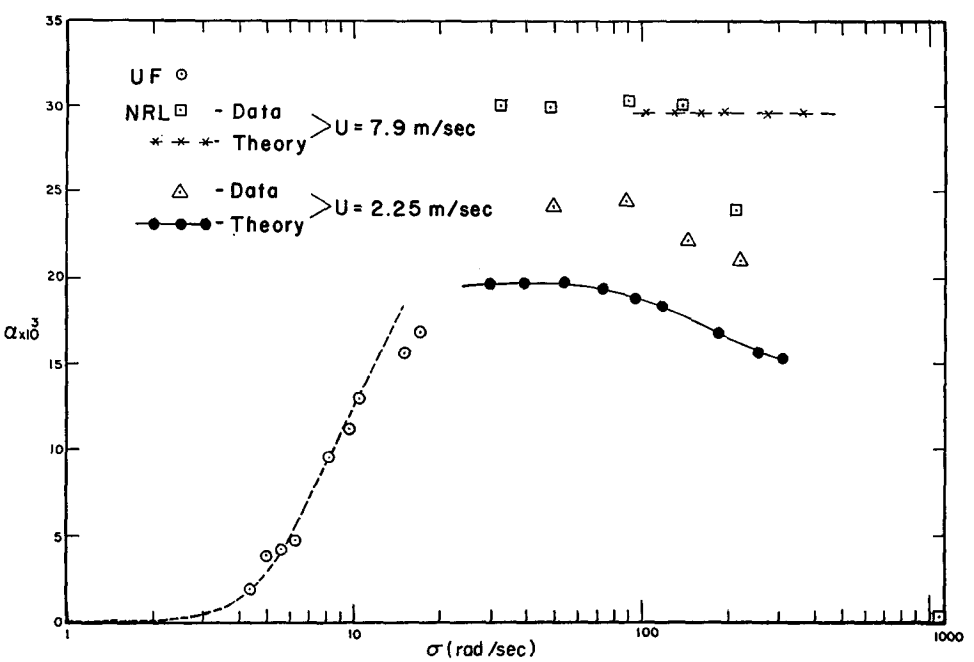

FIG. 6. Dependence of α on σ and U_∞ from numerical and experimental results.

TABLE 1. Comparison between computed and measured phase speed.

k (cm^{-1})	U_∞ (m sec^{-1})	Computed C_c (cm sec^{-1})	Measured C_m (cm sec^{-1})	Percent difference
1.90	7.9	51.4	51.6	−0.4
3.86	7.9	49.1	48.0	2.2
5.80	7.9	50.5	49.2	2.6
9.07	7.9	53.7	47.0	12.5
15.80	7.9	61.7	50.0	19.0
1.86	2.25	32.15	30.0	6.7
3.98	2.25	30.3	29.5	2.6
5.90	2.25	30.6	30.0	2.0
9.00	2.25	33.5	32.0	4.5
15.70	2.25	38.4	32.0	16.5

occurred in the computations. Modification of the numerical procedures appears to be necessary to extend the computations to the lower wavenumbers.

By way of summarizing the experimental and numerical results it was found convenient to parameterize the phase speed of waves in a shear flow according to

$$C=C_0+\alpha U_\infty, \tag{27}$$

where α is a shear flow parameter which can be dependent on U and wave frequency σ. Fig. 6 shows the dependence of α on σ for the experimental results described in this paper (denoted by UF) and the experimental results of Wright and Keller (1971) (denoted by NRL). Numerical computations for $U_\infty=2.25$ and 7.9 m sec^{-1} are also shown. The following observations are drawn under laboratory conditions:

1) When the surface drift is small or equal to the orbital wave velocity, the motion in water is dominated by the orbital motion and a negligible increase in phase speed is produced by the wind-induced drift.

2) When the surface drift is large compared to the orbital wave velocity, the surface wave is simply advected by the drift.

3) When the surface drift is of the same order of magnitude or slightly larger than the orbital velocity, a noticeable increase in phase speed can be expected.

The factor α represents the relative influence of the wind-induced drift on the phase speed of waves. It is observed that in the laboratory the wind-induced drift is large enough to produce a significant increase in phase speeds of capillary waves. In the field where wind speeds >100 mph are found under hurricane conditions a significant increase in phase speeds of gravity waves are to be expected.

5. Conclusions

The following conclusions are derived from this investigation:

1. The dispersion relationship governing small-amplitude waves is significantly altered by the wind-induced surface drift when the surface drift is large compared to the orbital wave velocity.

2. Strong interaction can exist between waves and the surface drift when the latter is not small. This can play a significant role in energy transfer among waves with different wavenumbers in a spectrum.

3. The wind-induced drift profile can be conveniently approximated by a logarithmic distribution.

4. When extending the above results to the open sea conditions care must be exercised to allow for the absence of lateral constraints.

Acknowledgments. The author acknowledges the contribution of Dr. A. Verma in the early phase of the numerical study and the efforts of Messrs. P. M. Lin and C. Hortsman in the experimental phase of the study. The research was supported by the National Science Foundation under Grant GK-3986 and the Coastal Engineering Research Center under Contract DACW 72-71-C-0020. Significant interaction with Dr. J. W. Wright at the Naval Research Laboratory facilitated parts of this study. His results were presented as a companion paper at the Conference on the Interaction of the Sea and the Atmosphere.

REFERENCES

Bye, J. A. T., 1967: The wave-drift current. *J. Marine Res.*, **25**, 95–102.

Conte, S. D., and J. W. Miles, 1959: On the numerical integration of the Orr-Sommerfeld equation. *J. Soc. Ind. Appl. Math.*, **7**, 361–366.

Cox, C. S., 1958: Measurements of slopes of high-frequency wind waves. *J. Marine Res.*, **16**, 199–225.

Francis, J. R. D., 1951: The aerodynamic drag of a free water surface. *Proc. Roy. Soc. London*, **A206**, 387–408.

Hide, G. M., and E. J. Plate, 1966: Wind action on water standing in a laboratory wave channel. *J. Fluid Mech.*, **26**, 651–687.

Huang, N. E. 1970: Mass transport induced by wave motion. *J. Marine Res.*, **20**, 35–50.

Kenyon, K. E., 1969: Stokes drift for random gravity waves. *J. Geophys. Res.*, **74**, 6991–6994.

Keulegan, G. H., 1951: Wind tides in small closed channels. *J. Res. Natl. Bur. Stnds.*, **46**, 358–391.

Lai, R. J., and O. H. Shemdin, 1971: Laboratory investigation of air turbulence above simple water waves. *J. Geophys. Res.*, **76**, 7334–7350.

Longuet-Higgins, M. S., 1960: Mass transport in the boundary layer at a free oscillating surface. *J. Fluid Mech.*, **8**, 293–306.

Miles, J. W., 1957: On the generation of wave by turbulent wind. *J. Fluid Mech.*, **2**, 417–445.

Plate, E., and M. Trawle, 1970: A note on the celerity of wind waves on a water current. *J. Geophys. Res.*, **75**, 3537–3544.

Saeger, J. C., and W. C. Reynolds, 1971: Perturbation pressures over traveling sinusoidal waves with fully developed turbulent shear flow. Tech. Rept. FM-9, Dept. of Mechanical Engineering, Stanford University.

Shemdin, O. H., 1969: Instantaneous velocity and pressure measurements above propagating waves. Tech. Rept. No. 4, Dept. of Coastal and Oceanographic Engineering, University Florida, Gainesville.

Van Dorn, W. G., 1953: Wind stress on an artificial pond. *J. Marine Res.*, **12**, 249–276.

Wright, J. W., and W. C. Keller, 1971: Doppler spectra in microwave scattering from wind waves. *Phys. Fluids*, **14**, 466–474.

Wu, J., 1968: Laboratory studies of wind wave interactions. *J. Fluid Mech.*, **34**, 91–122.